Supporting Information

Interwoven Carbon Nanotube Core-Shell Network Supports Co_9S_8-Ni_3S_2 Heterojunction for Superior Aqueous Nickel/Cobalt-Zinc Batteries Kinetics

Tao Zheng†[a], Zhiyu Song†[a], Jian Li[a], Yuyun Gao[a], Huiqi Jia[a], Xiaodan Xia[a], Zhenyu Xiao*[a], Lei Wang*[a]

a. Key Laboratory of Eco-chemical Engineering, Ministry of Education, International Science and Technology Cooperation Base of Eco-chemical Engineering and Green Manufacturing, College of Chemistry and Molecular Engineering, Qingdao University of Science and Technology, Qingdao 266042, P. R. China.

*Corresponding author.

† These authors contributed equally to this work.

E-mail: inorgxiaozhenyu@163.com (Zhenyu Xiao); inorchemwl@126.com (Lei Wang)

Experimental Section

Chemicals.

Cobalt nitrate hexahydrate [$Co(NO_3)_2 \cdot 6H_2O$, 98%] and potassium hydroxide [KOH, 85%] are purchased from Aladdin; nickel nitrate hexahydrate [$Ni(NO_3)_2 \cdot 6H_2O$, 98%], 1,3,5-benzenetricarboxylic acid [BTC, 99%] and thioacetamide [C_2H_5NS, 99%] are acquired from Energy Chemical; ethanol [C_2H_5OH, 95%] and ethylene glycol are gained from Sinopharm; carbon nanotube, carbon black and polytetrafluoroethylene [PTFE, 60%] are provided by Power source battery sales department. All chemical reagents are directly used without further experiment of purification.

Experimental

Synthesis of CoNi-BTC with various Co/Ni ratios: A series of bimetallic CoNi-BTC precursors with different Co/Ni molar ratios were synthesized via a solvothermal method. The sample with a Co/Ni ratio of 3:7 is denoted as CoNi-BTC. In its typical synthesis, $Co(NO_3)_2 \cdot 6H_2O$ (0.9 mmol), $Ni(NO_3)_2 \cdot 6H_2O$ (2.1 mmol), and 1,3,5-benzenetricarboxylic acid (H_3BTC, 285.8 mg) were dissolved in a mixed solvent of ethanol (160 mL) and ethylene glycol (240 mL). The mixture was ultrasonicated for homogenization, transferred to a Teflon-lined stainless-steel autoclave, and heated at 150 °C for 24 h. The resulting solid product was collected by centrifugation, washed several times with ethanol, and dried at 60 °C. For comparative studies, precursors with Co/Ni ratios of 2:8 and 4:6 were synthesized using identical procedures, with the molar amounts of $Co(NO_3)_2 \cdot 6H_2O$ and $Ni(NO_3)_2 \cdot 6H_2O$ adjusted to 0.6/2.4 mmol and 1.2/1.8 mmol, respectively. These are denoted as CoNi-BTC-2:8 and CoNi-BTC-4:6.

Synthesis of CoNi-CNT: The as-prepared CoNi-BTC precursor was calcined in a tube furnace at 800 °C for 2 h under a continuous N_2 atmosphere, yielding the carbon nanotube-embedded intermediate denoted as CoNi-CNT. Using the same pyrolysis conditions, the corresponding intermediates derived from CoNi-BTC-2:8 and CoNi-

BTC-4:6 were obtained and are denoted as CoNi-CNT-2:8 and CoNi-CNT-4:6, respectively.

Synthesis of CoNiS/CNT: The CoNiS/CNT composite was obtained via a solvothermal sulfidation process. Specifically, the CoNi-CNT intermediate (50 mg) was dispersed in 10 mL of ethanol. Separately, thioacetamide (25 mg) was dissolved in 5 mL of ethanol. After individual ultrasonication, the two solutions were combined, further ultrasonicated, and then transferred to a Teflon-lined autoclave to react at 180 °C for 12 h. The product was collected by centrifugation, washed with ethanol, and vacuum-dried. Using the identical sulfidation procedure but starting with the CoNi-CNT-2:8 and CoNi-CNT-4:6 intermediates, the corresponding composites CoNiS/CNT-2:8 and CoNiS/CNT-4:6 were synthesized.

Synthesis of CoNi-BTC-S: For comparison, a control sample CoNi-BTC-S was synthesized by subjecting the original CoNi-BTC precursor to the same solvothermal sulfidation process. Specifically, CoNi-BTC (100 mg) was dispersed in 10 mL of ethanol, and thioacetamide (25 mg) was dissolved in 5 mL of ethanol. Both mixtures were ultrasonicated individually, combined, and ultrasonicated again. The homogeneous mixture was then transferred to a Teflon-lined autoclave and reacted at 180 °C for 12 h. The final product was isolated by centrifugation, washed with ethanol, and vacuum-dried.

Synthesis of CoNiS: The CoNiS sample was prepared by first calcining the CoNi-BTC precursor in air at 600°C for 2 h to obtain metal oxides, followed by the same sulfidation process used for CoNiS/CNT.

Synthesis of CoS/CNT and NiS/CNT: Co-BTC and Ni-BTC precursors were first synthesized via a solvothermal method similar to that of CoNi-BTC, using $Co(NO_3)_2 \cdot 6H_2O$ or $Ni(NO_3)_2 \cdot 6H_2O$ as the sole metal source, respectively. Each precursor was then pyrolyzed at 800°C for 2 h under N_2 atmosphere to obtain Co-CNT and Ni-CNT intermediates. Finally, these intermediates were subjected to the same

solvothermal sulfidation process as used for CoNiS/CNT (thioacetamide in ethanol at 180 °C for 12 h), yielding the final CoS/CNT and NiS/CNT composites.

Materials characterization:

The surface morphology and microstructure of the samples are studied by scanning electron microscopy (SEM, JEOL, Zeiss merlin) and transmission electron microscopy (TEM, FEI Tecnai G^2 F20). The phase and crystal structure are characterized by X-ray diffraction (XRD, Rigaku D-MAX2500/PC) with Cu-Kα radiation (λ = 1.5418 Å). The test range of XRD is 5°-80° and the rate is 5° min^{-1}. And the elemental composition and valence states are studied by X-ray photoelectron spectroscopy (XPS, Thermo Scientific 250xl).

Electrochemical measurements:

Three-electrode system tests: All three-electrode electrochemical tests were performed in 6 M KOH aqueous electrolyte at room temperature. The three-electrode setup consisted of a Hg/HgO reference electrode, a platinum wire counter electrode, and the as-prepared working electrode. The working electrode was fabricated by homogeneously mixing the active material, carbon black, and PTFE (5%) at a mass ratio of 8:1:1 in a small volume of ethanol. The mixture was dried under vacuum at 60°C overnight to remove residual solvent. Subsequently, 2.5 mg of the resulting solidified mixture (containing 2.0 mg of active material) was carefully placed between two pieces of nickel foam (each 2×1 cm^2), ensuring a loading area of 1×1 cm^2. The assembly was then pressed at 10 MPa for 5 seconds to ensure electrical contact and mechanical stability.

Two-electrode full-cell tests: The electrochemical performance of Zn//CoNiS/CNT battery was evaluated using a two-electrode system. The cathode was

fabricated following the same procedure as described for the three-electrode working electrode. Specifically, 2.5 mg of the resulting solidified mixture (containing 2.0 mg of active material) was carefully placed between two pieces of nickel foam (each 2×1 cm^2), ensuring a loading area of 1×1 cm^2. A zinc plate (2×1 cm^2) served as the anode, with an effective area of 1×1 cm^2 in contact with the electrolyte. A mixed solution of 6 M KOH and 0.2 M $Zn(CH_3COO)_2$ was used as the electrolyte. CV and GCD tests were conducted in the voltage range of 1.4-1.9 V at room temperature. Long-term cycling performance was tested at a current density of 20 mA cm^{-2} using the same Landian battery testing system. All specific capacity values reported for the full-cell are normalized to the mass of the active material (2.0 mg) on the cathode.

Cyclic voltammetry (CV) and galvanostatic charge/discharge (GCD) tests were conducted using an electrochemical workstation (DONGHUA DH7000, Jiangsu Donghua Instrument Co., China) in the voltage range of 0-0.5 V (*vs.* Hg/HgO). Electrochemical impedance spectroscopy (EIS) and phase angle tests were performed on a CHI 660E electrochemical workstation (CHI 660E, Shanghai Chenhua Instrument Co., China). During the stepwise charge/discharge process, EIS measurements were acquired across a frequency range of 0.1-100 kHz with an amplitude of 5 mV under open-circuit potential conditions, with measurements taken at voltage increments of 0.1 V during both charging and discharging. The distribution of relaxation times (DRT) was extracted from the EIS data to resolve the underlying electrochemical processes in the CoNiS/CNT electrode. Long-term cycling stability was evaluated using a Landian battery testing system (CT2001A, Wuhan Landian, China). For three-electrode tests, the cycling current density was 20 mA cm^{-2} within the voltage range of 0-0.5 V (*vs.* Hg/HgO).

Soft-packaged Device Fabrication:

The soft-packaged device was assembled using the following components: an aluminum-plastic laminate film pouch, positive electrode, negative electrode, a separator, electrolyte, and two nickel tabs. Two square pieces of aluminum-plastic

laminate film (5×5 cm^2) were used to form the hermetic pouch casing.

The positive electrode was fabricated following the same procedure as described for the two-electrode system. Specifically, 2.5 mg of the solidified mixture (containing 2.0 mg of CoNiS/CNT active material) was loaded onto a nickel foam substrate (2×1 cm^2) with an effective loading area of 1×1 cm^2. A zinc plate (2×1 cm^2) served as the anode, with an effective area of 1×1 cm^2 in contact with the electrolyte A filter paper separator (3×3 cm^2) was inserted between the two electrodes to prevent direct electrical contact and mitigate short-circuit risks. Two nickel tabs were securely attached to the positive and negative electrodes, with their terminals partially exposed outside the pouch casing for connection to the external circuit. Prior to sealing, 100 μL of electrolyte (6 M KOH with 0.2 M $Zn(CH_3COO)_2$) was added to wet the electrodes and separator. The pouch was then heat-sealed, completing the fabrication of the flexible soft-packaged battery.

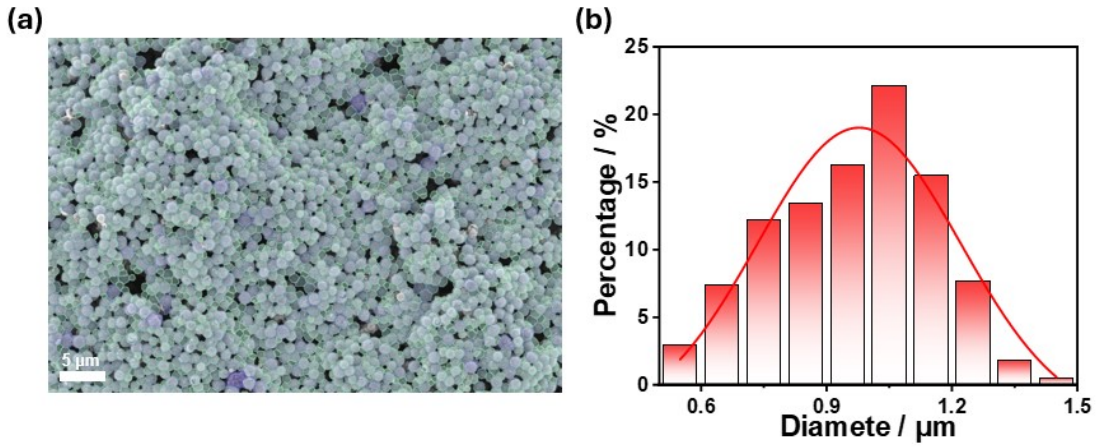

Figure S1. (a) Low-resolution SEM images and (b) particle size distribution diagrams of CoNi-BTC.

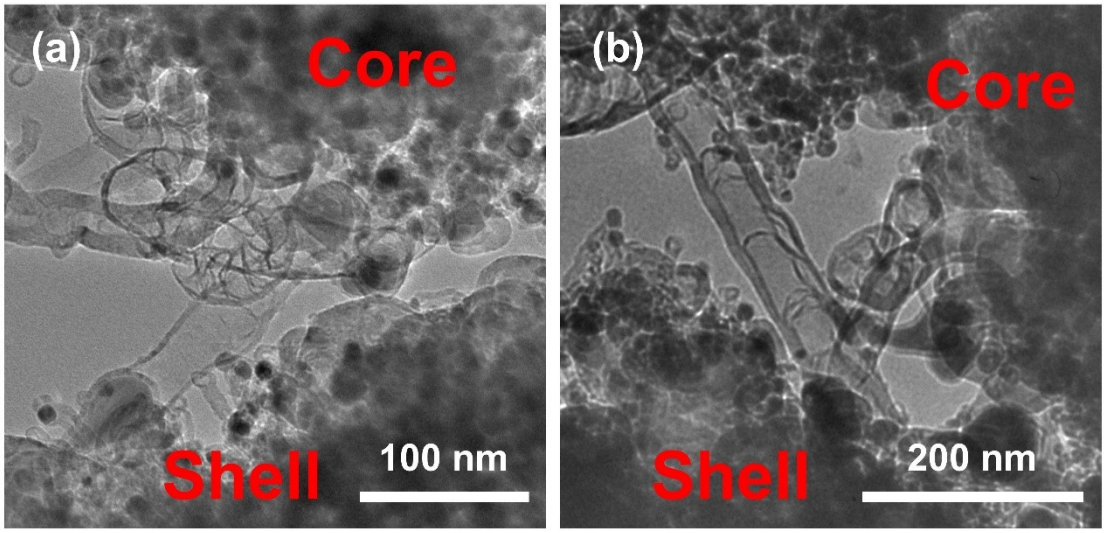

Figure S2. (a, b) TEM image of CoNiS/CNT showing interwoven CNTs bridging the core–shell gap.

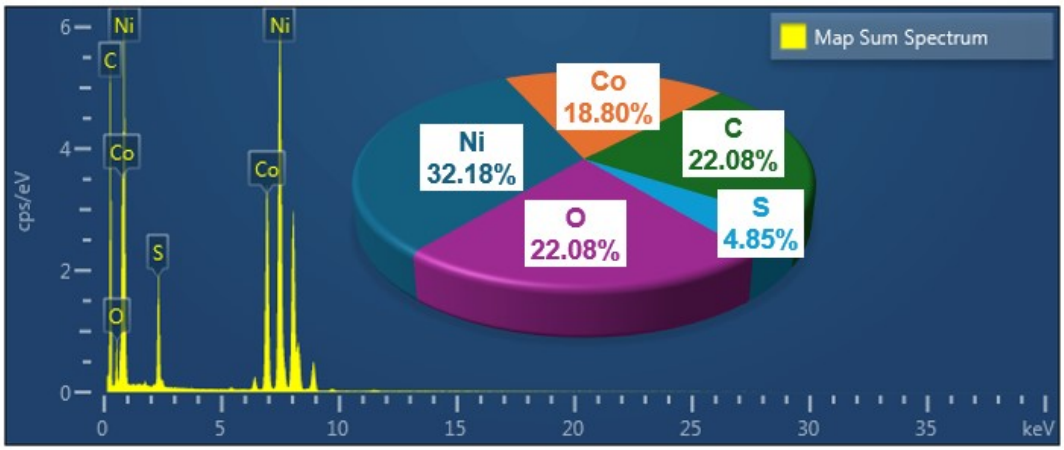

Figure S3. The EDS spectra of CoNiS/CNT.

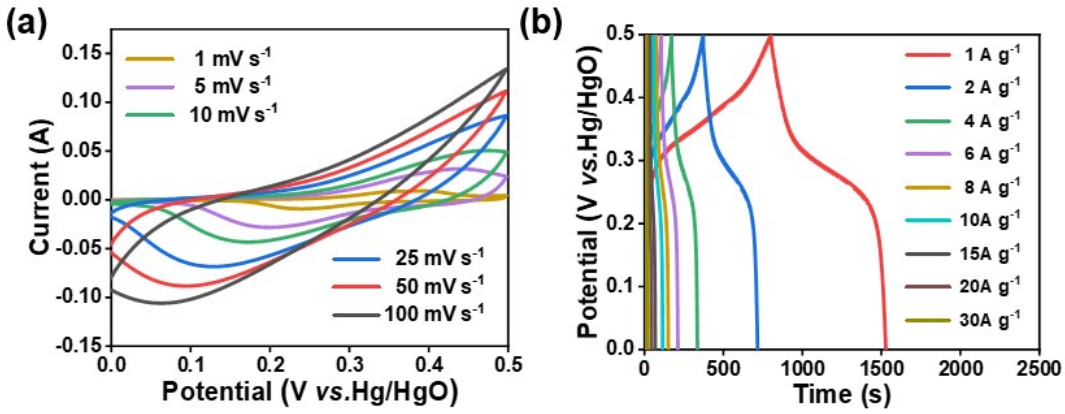

Figure S4. (a) CV curves and (b) GCD curves of CoNiS/CNT.

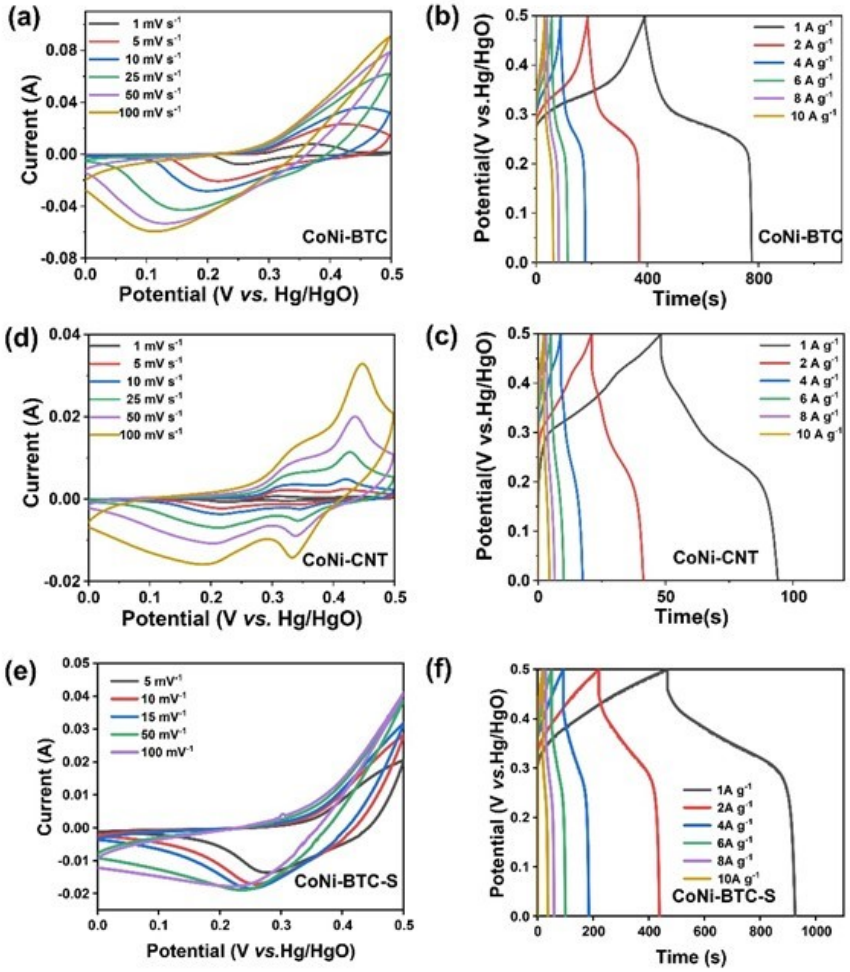

Figure S5. (a) CV curves (b) GCD curves of CoNi-BTC; (c) CV curves (d) GCD curves of CoNi-CNT; (e) CV curves (f) GCD curves of CoNi-BTC-S.

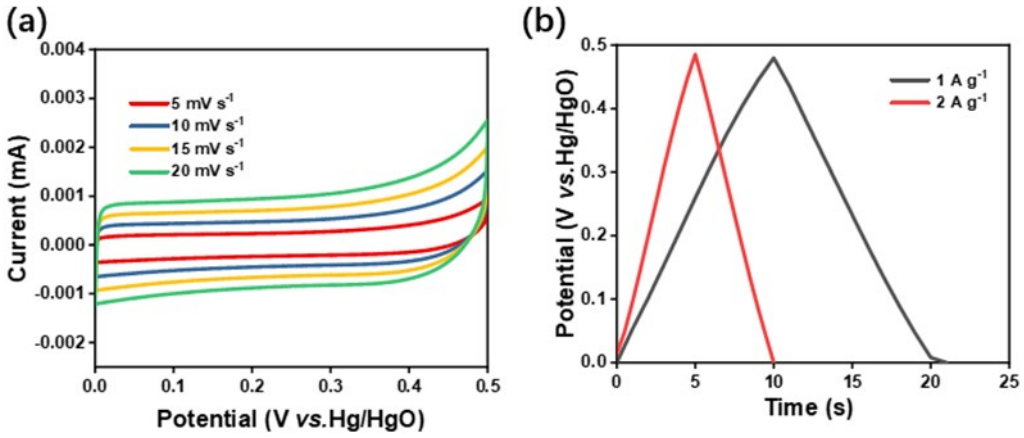

Figure S6. (a) CV curves and (b) GCD curves of CNT.

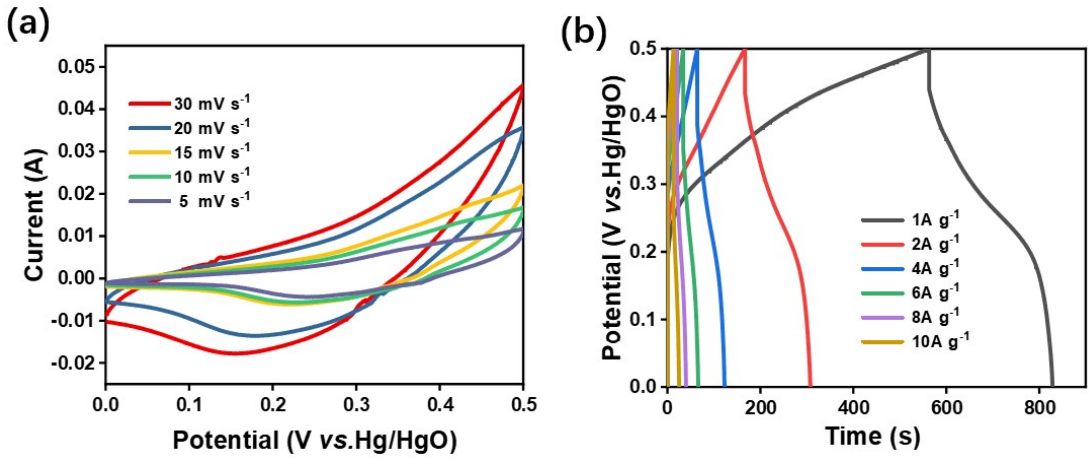

Figure S7. (a) CV curves and (b) GCD curves of Co_9S_8-Ni_3S_2.

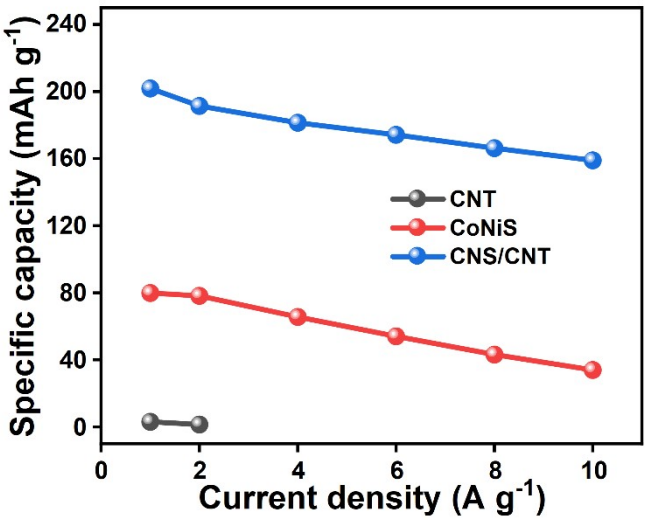

Figure S8. Specific capacities under different current densities of CNT, CoNiS and CoNiS/CNT.

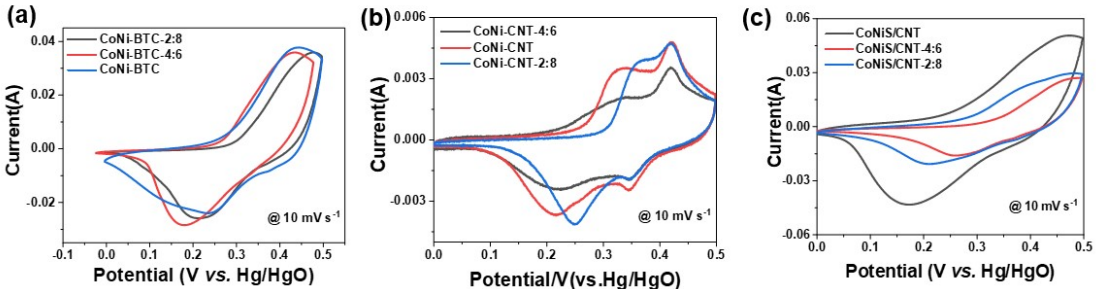

Figure S9. (a) CV curves of CoNi-BTC-2:8, CoNi-BTC and CoNi-BTC-4:6 at scan rate of 10 mV^{-1}. (b) CV curves of CoNi-CNT-2:8, CoNi-CNT and CoNi-CNT-4:6 at scan rate of 10 mV^{-1}. (c) CV curves of CoNiS/CNT-2:8, CoNiS/CNT and CoNiS/CNT-4:6 at scan rate of 10 mV^{-1}.

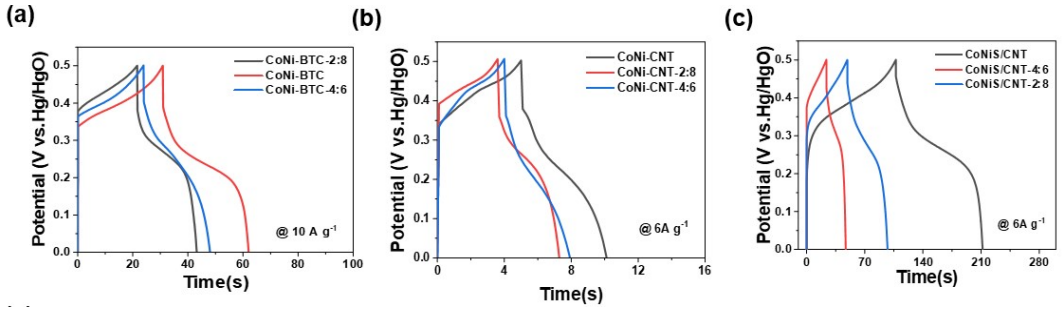

Figure S10. (a) GCD curves of CoNi-BTC-2:8, CoNi-BTC and CoNi-BTC-4:6 at current density of 6 A g^{-1}. (b) GCD curves of CoNi-CNT-2:8, CoNi-CNT and CoNi-CNT-4:6 at current density of 6 A g^{-1}. (c) GCD curves of CoNiS/CNT-2:8, CoNiS/CNT and CoNiS/CNT-4:6 at current density of 6 A g^{-1}.

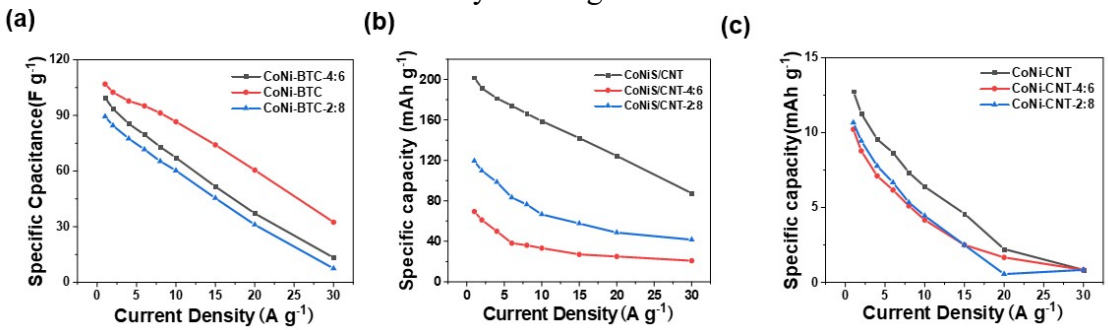

Figure S11. (a) Specific capacities under different current densities of CoNi-BTC-2:8, CoNi-BTC and CoNi-BTC-4:6. (b) Specific capacities under different current densities of CoNi-CNT-2:8, CoNi-CNT and CoNi-CNT-4:6. (c) Specific capacities under different current densities of CoNiS/CNT-2:8, CoNiS/CNT and CoNiS/CNT-4:6.

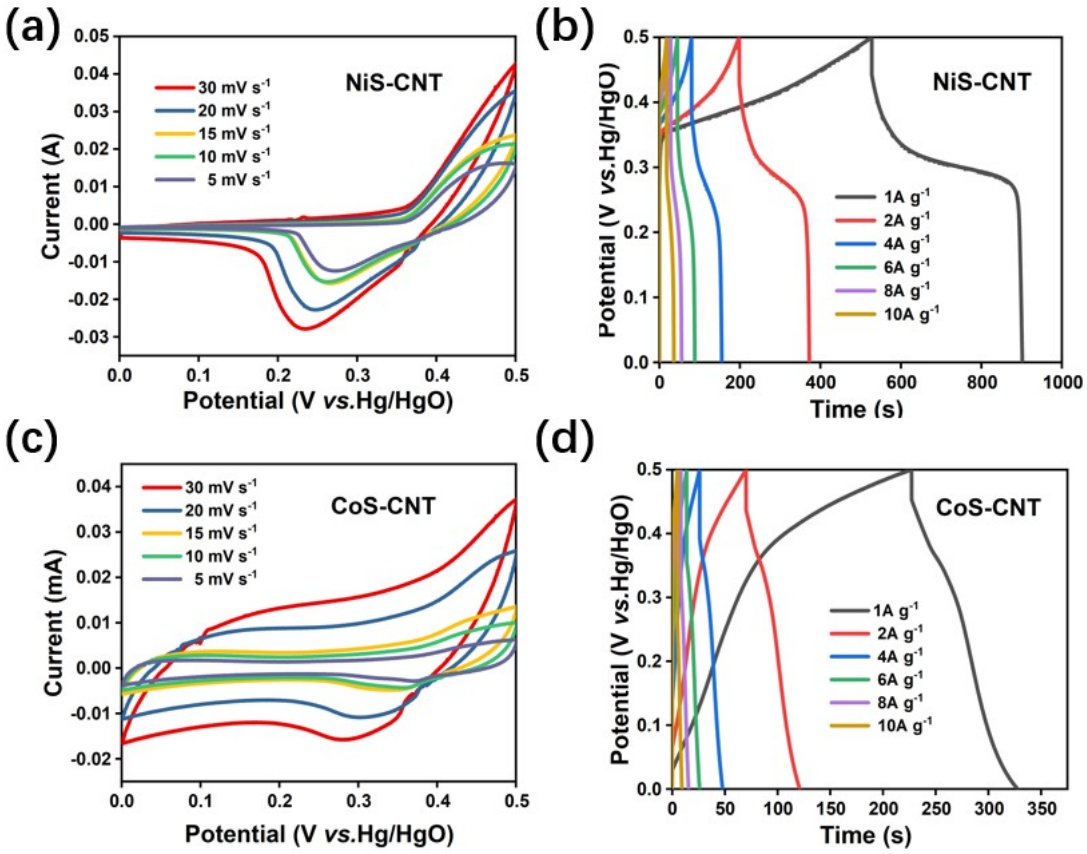

Figure S12. (a) CV curves and (b) GCD curves of Ni-CNT; (c) CV curves and (d) GCD curves of CoS-CNT.

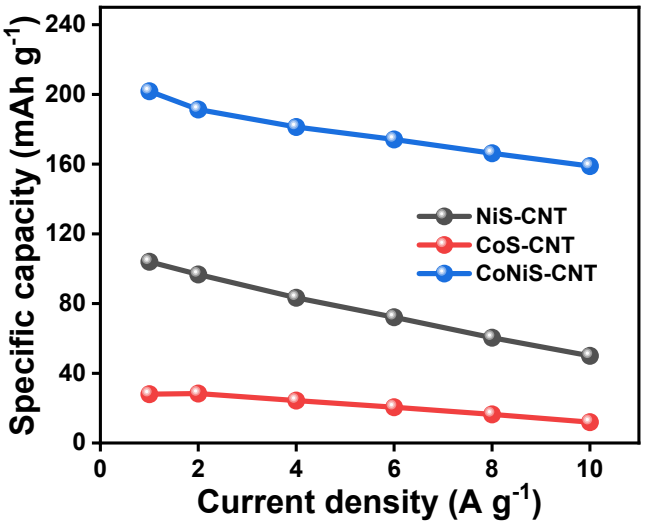

Figure S13. Specific capacities under different current densities of NiS-CNT, CoS-CNT and CoNiS/CNT.

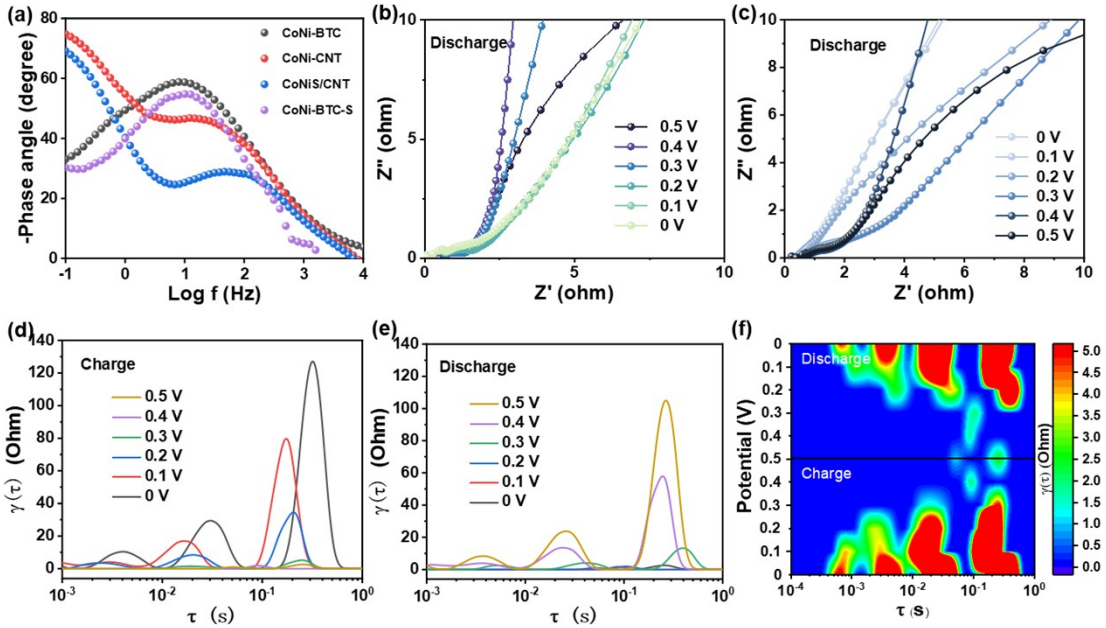

Figure S14. (a) the Bode phase plots of CoNi-BTC, CoNi-CNT, CoNiS/CNT and CoNi-BTC-S. EIS curves during discharge process of (b) CoNiS/CNT and (c) CoNi-BTC-S. (d), (e) DRT plot during charge–discharge process of CoNi-BTC-S. (f) The contour plots of corresponding DRT at charge–discharge processes.

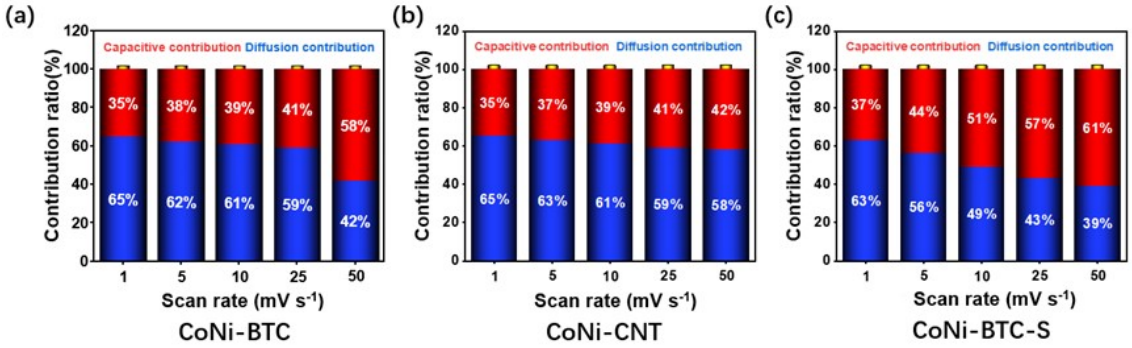

Figure S15. Capacitive contribution analysis of CoNi-BTC, CoNi-CNT and CoNi-BTC-S.

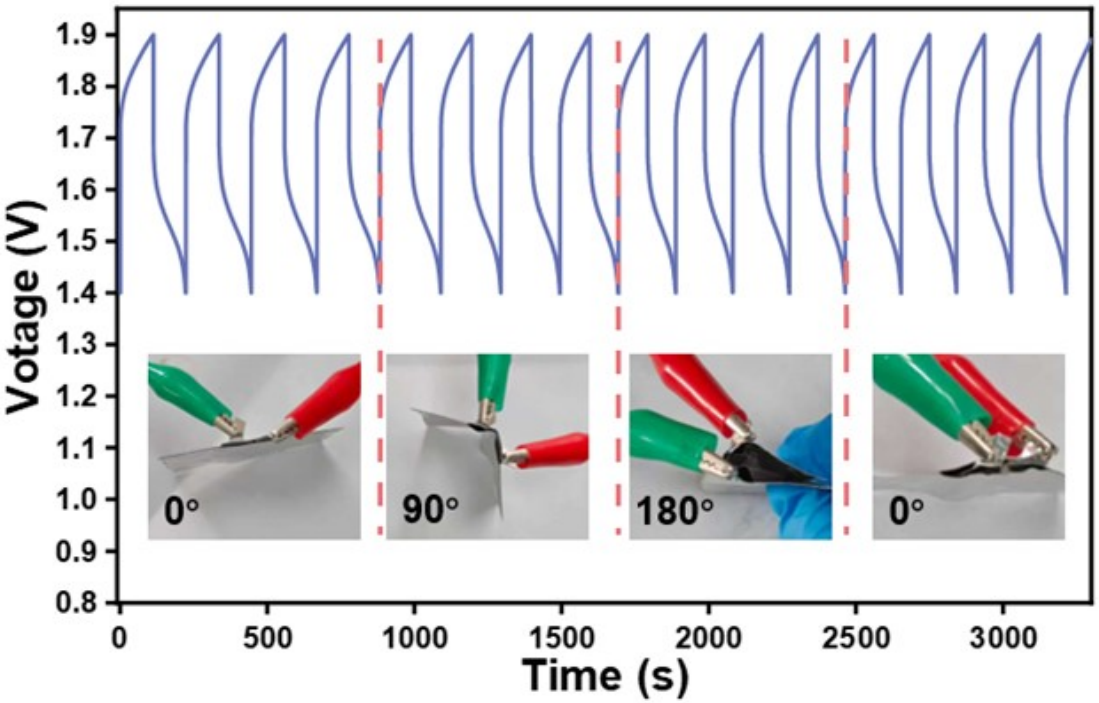

Figure S16. Cycle performance of 6 A g^{-1} of flexible device under simulated varying degree of bending test.

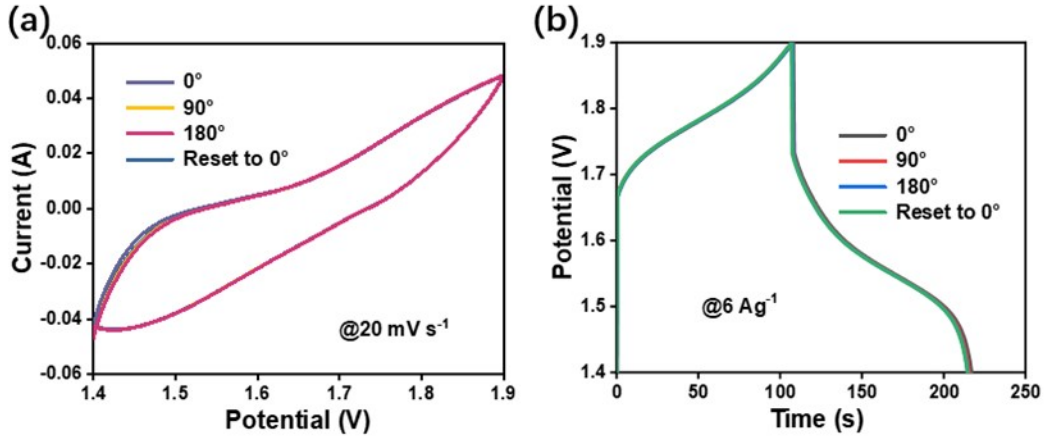

Figure S17. The CV curves at 20 mV s^{-1} of and (b) GCD curves of 6 A g^{-1} of Zn//CoNiS/CNT at different bending angles.

Table S1 Parameters of the proposed equivalent circuit model.

Elements / Samples	Rs (Ω)	Rct (Ω)	CPE-T (F)	CPE-P	W-R (Ω)	W-T	W-P
CoNi-BTC	0.5482	63.57	0.0089	0.7412	160.4	70.8	0.371
CoNi-CNT	0.6351	1.100	0.0031	0.8113	32.17	0.362	0.447
CoNiS/CNT	0.6144	1.266	0.0044	0.8183	5.569	0.276	0.418
CoNi-BTC-S	0.7288	23.19	0.0080	0.8070	387.6	122.8	0.553

Table S2 Comparison of NiCo//Zn battery performance with the other works.

Year	Sample	Power density ($kW\ kg^{-1}$)	Energy density ($Wh\ kg^{-1}$)	Ref.
2020	Zn//$NiCo_2O_4$@NiMn LDH	1.6	234.5	[38]
2022	Zn//NiCo-S-2/RGO	1.7	333.2	[39]
2022	Zn//$NiCoO_2$@N-C	0.7	226.1	[40]
2023	Zn//CC@NC-$NiCo_2S_4$	1.3	238	[41]
2025	Zn//FePc/CoNi-LDH	1.4	327.8	[42]
2025	rGO-Zn//Cu_2S/CoNi-LDH@C	0.45	254.7	[43]
2025	Zn//MBene-NCBM	3.3	280	[44]
2026	Zn//CoNiS/CNT	1.6	343.2	This work

All specific capacity values reported for the full-cell are normalized to the mass of the active material on the cathode.

Equation:

The electrochemical reaction of Zn//CoNiS/CNT in the alkaline electrolyte is:

Cathode reactions:

$$Co_9S_8 + xOH^- \rightleftharpoons Co_9S_8(OH)_x + xe^-$$

..... Equation S1-1

$$Ni_3S_2 + xOH^- \rightarrow Ni_3S_2(OH)_x + xe^-$$

..... Equation S1-2

Anode reactions:

$$Zn + 4OH^- \rightleftharpoons Zn(OH)_4^{2-} + 2e^-$$

..... Equation S2

$$Q = \frac{I\Delta t}{m \times 3.6}$$

..... Equation S3

Where Q (mAh g^{-1}) is the specific capacity, I (mA) is the discharge current, Δt (s) is the discharge time, m (mg) is the mass of the active material, and the factor 3.6 is the unit conversion coefficient (3600/1000) for converting seconds to hours and milligrams to grams.

The voltage window for all GCD measurements was 0-0.5 V (*vs.* Hg/HgO) for three-electrode tests and 1.4-1.9 V for full-cell tests.

$$D = \frac{RT^2}{2A^2n^4F^4C^2R\sigma^2}$$

.....Equation S4

Where R (J mol^{-1} K^{-1}), T (K), A (cm^{-2}), n, F (C mol^{-1}), C (L mol^{-1}) and σ are the gas constant, absolute temperature, reaction area of electrode, quantity of transferred electrons, Faraday constant, concentration of electrolyte and Warburg diffusion coefficient, respectively.

$$Z = R_s + R_{ct} + \sigma\omega^{-\frac{1}{2}}$$

.....Equation S5

where ω (Hz), Z' (Ω) and Rs (Ω) are angular frequency, reactance and internal resistance, respectively.

The DRT-impedance, $Z_{DRT}(f)$, at a frequency f, is expressed EIS as

$$Z_{DRT}(f) = i2\pi f L_0 + R_\infty + \int_{-\infty}^{+\infty} \frac{\gamma(log\tau)}{1 + i2\pi f\tau} dlog\tau$$

.....Equation S6

where L_0, R_∞, τ, and $\gamma(log\tau)$ denote the inductance, ohmic resistance, timescale, and DRT function, respectively. The total polarization resistance (R_{pol}) was computed via:

$$R_{pol} = \int_{-\infty}^{+\infty} \gamma(log\tau) dlog\tau$$

.....Equation S7

$$i = k_1 v^{1/2} + k_2 v$$

..... Equation S8

Where i and v stand for the peak current density and scan rate, respectively. Generally, $k_1 v^{1/2}$ and $k_2 v$ are associated with the bulk process contribution and the surface process contribution of the peak current density, respectively.

$$E = \frac{I}{m} \int_{t2}^{t_1} V$$

.....Equation S9

Where E is the energy density (Wh kg^{-1}), and V (V) is the discharge voltage.

$$P = \frac{E}{\Delta t}$$

.....Equation S10

Where P is the power density (kW kg^{-1}), E is the energy density (Wh kg^{-1}), Δt is the discharging time.